# Induction of store operated calcium entry (SOCE) suppresses glioblastoma growth by inhibiting the Hippo pathway transcriptional coactivators YAP/TAZ

**Zhijun Liu**[1], **Yiju Wei**[1], **Lei Zhang**[1,5], **Patricia P. Yee**[1], **Martin Johnson**[2], **Xuexin Zhang**[2], **Melissa Gulley**[1], **Jennifer Xavier**[1], **Mohamed Trebak**[2], **Hong-Gang Wang**[1,3], and **Wei Li**[1,4,*]

[1]Division of Pediatric Hematology/Oncology, Department of Pediatrics, Penn State Health Hershey Medical Center, Penn State College of Medicine, Hershey, PA 17033

[2]Department of Cellular & Molecular Physiology, Penn State Health Hershey Medical Center, Penn State College of Medicine, Hershey, PA 17033

[3]Department of Pharmacology, Penn State Health Hershey Medical Center, Penn State College of Medicine, Hershey, PA 17033

[4]Department of Biochemistry & Molecular Biology, Penn State Health Hershey Medical Center, Penn State College of Medicine, Hershey, PA 17033

[5]Hepatic Surgery Center, Tongji Medical College, Huazhong University of Science and Technology, Wuhan, China

## Abstract

Glioblastomas (GBM) are the most aggressive brain cancers without effective therapeutics. The Hippo pathway transcriptional coactivators YAP/TAZ were implicated as drivers in GBM progression and could be therapeutic targets. Here, we found in an unbiased screen of 1650 compounds that amlodipine is able to inhibit survival of GBM cells by suppressing YAP/TAZ activities. Instead of its known function as an L-type calcium channel blocker, we found that amlodipine is able to activate $Ca^{2+}$ entry by enhancing store-operated $Ca^{2+}$ entry (SOCE). Amlodipine as well as approaches that cause store depletion and activate SOCE trigger phosphorylation and activation of Lats1/2, which in turn phosphorylate YAP/TAZ and prevent their accumulation in the cell nucleus. Furthermore, we identified that protein kinase C (PKC) beta II is a major mediator of $Ca^{2+}$-induced Lats1/2 activation. $Ca^{2+}$ induces accumulation of PKC beta II in an actin cytoskeletal compartment. Such translocation depends on inverted formin-2 (INF2). Depletion of INF2 disrupts both PKC beta II translocation and Lats1/2 activation. Functionally, we found that elevation of cytosolic $Ca^{2+}$ or PKC beta II expression inhibits YAP/TAZ-mediated gene transcription. In vivo PKC beta II expression inhibits GBM tumor growth and prolongs mouse survival through inhibition of YAP/TAZ in an orthotopic mouse xenograft model. Our studies

*Corresponding Author: Wei Li, Ph.D., Department of Pediatrics, Penn State Hershey College of Medicine, 500 University Drive, PO Box 850, MC H085, Hershey, PA 17033, Phone: 717-531-0003 ×282050, Fax: 717-531-4789, weili@pennstatehealth.psu.edu.

Conflict of Interest statement
There is no conflict of interest to disclose.

indicate that $Ca^{2+}$ is a crucial intracellular cue that regulates the Hippo pathway, and that triggering SOCE could be a strategy to target YAP/TAZ in GBM.

## Introduction

Glioblastomas (GBM) are the most aggressive brain cancers. Median survival of patients with GBM is only 12–17 months [1]. Currently, surgery followed by radiotherapy and chemotherapy is still the major treatment, although the outcome is usually poor. Development of targeted therapies for these cancers based on oncogenic mutations and signaling pathways could alter the prognosis. Integrated genomic and gene expression signature studies classified GBM into several subtypes differing in treatment responses and survival rates [2, 3]. Among these subtypes, the mesenchymal group associates with worst prognosis [2]. Gene regulatory network analysis and comprehensive analysis of brain tumor samples by immunohistochemistry found transcriptional coactivator with PDZ-binding motif (TAZ) and Yes-associated protein (YAP), as drivers in GBM mesenchymal transformation [4, 5].

YAP and TAZ (YAP/TAZ) are two paralogous nuclear effectors of the Hippo signaling pathway, which is a conserved signalling network governing cellular growth and survival [6]. This pathway contains a core serine/threonine kinase cascade, including MST1/2 kinases and their substrates Lats1/2 kinases. The upstream growth control signals from cell-cell contact, cell-matrix contact, extracellular soluble factors, as well as intracellular metabolic levels can lead to activation of Lats1/2, which in turn phosphorylate and inhibit YAP/TAZ by preventing their accumulation in the nucleus. The Hippo pathway thus suppresses the downstream oncogenic transcription and promotes quiescence. Loss of this growth control machinery could lead to enlarged organs and even tumorigenesis due to cell hyperproliferation and dysfunctional cell removal via apoptosis. Consistently, YAP/TAZ activation is widely found in multiple human cancers [7, 8]. Recent studies have also found that hyperactivation of YAP/TAZ is associated with resistance to canonical chemotherapies, radiotherapies and targeted therapies [9–12]. Therefore, drugs targeting YAP/TAZ have been of recent interest in cancer treatment [13].

$Ca^{2+}$ is a fundamental intracellular signal that regulates a variety of cellular functions. Elevation of cytosolic $Ca^{2+}$ ($[Ca^{2+}]_i$) could paradoxically promote both cell proliferation and cell death. It has long been realized that cancer cells hijack the $Ca^{2+}$-signaling toolkit to benefit their proliferation and migration; therefore targeting $Ca^{2+}$ transport has been proposed for cancer treatment [14]. On the other hand, cancer cells also develop strategies to avoid $Ca^{2+}$-induced cell death; and these strategies may also be explored for cancer therapies [15]. SOCE is the most ubiquitous $Ca^{2+}$ signaling pathway in non-excitable cells. It is activated upon depletion of the internal $Ca^{2+}$ reserves of the endoplasmic reticulum (ER) [16]. The activation process involves sensing of $Ca^{2+}$ store depletion by the ER protein STIM1, which aggregates in ER-plasma membrane junctional areas to trap and activate the SOCE channel, formed by Orai proteins (Orai1–3) [17]. The STIM/Orai signaling nexus has been implicated in tumorigenesis and has been proposed to be a viable target for therapeutic interventions [18].

Here, we conducted an unbiased screen using a library containing 1650 compounds, most of which are FDA-approved drugs. From the screen, we found that amlodipine inhibits GBM cells survival by suppressing YAP/TAZ activities. Unexpectedly, we found that in addition to its canonical function as a L-type calcium channel blocker (LTCCB), amlodipine is able to activate $Ca^{2+}$ entry through SOCE via Orai channels. Thus, elevation of intracellular $Ca^{2+}$ inhibits YAP/TAZ by activating the core serine/threonine kinase cascade of the Hippo pathway. This process depends on INF2-mediated $Ca^{2+}$-induced actin remodeling and PKC beta II. Correspondingly, elevation of PKC beta II expression inhibits glioblastoma cell growth and tumorigenesis by inhibiting YAP/TAZ. We propose that the SOCE-PKC beta II axis could be used to inhibit YAP/TAZ-active GBM.

## Results

### Amlodipine inhibits survival of GBM cells by suppressing YAP/TAZ activities

YAP/TAZ are activated during the development of GBM. To identify methods of inhibiting GBM growth, we carried out a small molecule screen using a library containing 1650 compounds, most of which are FDA-approved drugs. Our screen used LN229 human GBM cell line, which shows increased expression of TAZ [19], presumably due to gene amplification (TCGA database). We confirmed that TAZ is essential for cell growth and tumorigenesis of LN229 cells by shRNA-mediated knockdown of TAZ in these cells (Figure S1A-S1F). From the screen, we found a set of L-type calcium channel blockers (LTCCBs) that can effectively inhibit the survival of these cells (Figure 1A). Among these LTCCBs, both amlodipine and amlodipine besylate show around 95% inhibition. We confirmed that amlodipine can inhibit LN229 cell survival at $IC_{50}=11\mu M$ (Figure 1B). We noted a discrepancy of amlodipine efficacy between the screen and this confirmation assay. This may be due to different amlodipine sources or dilution methods used in these different assays. We then examined the effects of amlodipine on YAP/TAZ and found that amlodipine induces YAP phosphorylation and reduces their expression levels in a dose-dependent manner after 24 hours of treatment (Figure 1C). To determine whether reduced expression levels of YAP/TAZ were a consequence of amlodipine-induced cell death, we conducted time course studies. We found that as little as ten minutes of amlodipine treatment can induce mild increase of YAP phosphorylation (Figure 1D). We also saw YAP/TAZ cytoplasmic translocation after as little as 30 minutes of treatment (Figure 1E). This cytoplasmic translocation was followed by inhibition of expressions of YAP/TAZ target genes CTGF and Cyr61 (Figure 1F). These results suggested that amlodipine induces YAP/TAZ phosphorylation, which may promote their degradation. To test this notion, we stably expressed TAZ[4SA] or YAP[5SA], which cannot be regulated by phosphorylation [20, 21]. Compared to the native forms, expression levels of both mutants appear to be less reduced by amlodipine (Figure S1G). However, amlodipine still reduces their expression, especially TAZ[4SA], at higher concentrations. This is probably due to the secondary effect of cell death or a phosphorylation-independent mechanism.

To examine if inactivation of YAP/TAZ accounted for the inhibition of cell survival by amlodipine, we assessed LN229 cells stably expressing the constitutively active mutant, TAZ[4SA] or YAP[5SA]. Cells expressing TAZ[4SA] or YAP[5SA] were less inhibited by amlodipine

(Figure 1G). Conversely, silencing TAZ expression by shRNAs made these cells more sensitive to amlodipine (Figure 1H). These results indicated that amlodipine inhibits the survival of LN229 cells by suppressing YAP/TAZ activities. We also examined the effects of amlodipine in normal human astrocytes (NHA) and found that it can also inhibit their survival similarly as LN229 cells (Figure S1H). Notably, amlodipine can also induce YAP/TAZ phosphorylation in NHA (see below).

## Amlodipine activates $Ca^{2+}$ entry through SOCE in LN229 cells

While contemplating how amlodipine, an LTCCB, could induce YAP/TAZ phosphorylation, we anticipated that amlodipine inhibits $Ca^{2+}$ entry thereby regulating YAP/TAZ. Surprisingly, we found that amlodipine increased cytosolic $Ca^{2+}$ in LN229 cells in a dose-dependent manner (Figure S2A). To further understand these unexpected effects on $Ca^{2+}$ signaling and since GBM cells are non-excitable cells, we considered that amlodipine could be activating SOCE. SOCE is a ubiquitous $Ca^{2+}$ entry pathway in non-excitable cells that is activated by luminal ER $Ca^{2+}$ store depletion. Following store depletion, the ER transmembrane proteins, STIM, aggregates and migrates towards the ER-plasma membrane junctions to trap and activate the plasma membrane pore-forming protein Orai to stimulate SOCE. There are three homologs of Orai (Orai1–3), and in most cells only Orai1 is necessary for SOCE [17]. There are few pharmacological inhibitors of SOCE that can be useful in identifying SOCE. These include the compound 2-Aminoethoxydiphenyl borate (2-APB), which at high concentrations (50μM) inhibits Orai1 and Orai2, but potentiates Orai3. The lanthanide ion $Gd^{3+}$, when used at relatively low concentrations (<5μM) is a relatively specific inhibitor of all Orai channels. The myosin-light-chain kinase (MLCK) inhibitor, ML-9 (at 50μM) inhibits STIM1 aggregation[22–26]. To characterize the SOCE pathway in LN229 cells, the ER internal stores were passively depleted using either thapsigargin (1 μM), a pharmacological inhibitor of the sarcoplasmic/endoplasmic reticulum $Ca^{2+}$ ATPase (SERCA) pump, or using relatively low microsomal concentrations of the $Ca^{2+}$ ionophore ionomycin (100 nM) [27, 28]. Intracellular $Ca^{2+}$ measurements were achieved using the ratiometric dye Fura2. Fura2 is excited alternately at 340 nm and 380 nm and fluorescence emission is collected at 510 nm. The ratio of Fura2 emission (F340/F380) upon excitation at 340nm (which increase on $Ca^{2+}$ binding) to its emission upon excitation at 380nm (which decrease on $Ca^{2+}$ binding) is directly proportional to the amount of cytosolic $Ca^{2+}$. Addition of either thapsigargin (Figure 2A) or ionomycin (Figure S2B) to LN229 cells in a nominally $Ca^{2+}$ free external bath solution caused a typical passive release of $Ca^{2+}$ from ER stores, reminiscent of widely documented $Ca^{2+}$ release signals in many non-excitable cell types. Subsequent restoration of $Ca^{2+}$ (2 mM) to the bath solution revealed the activation of the $Ca^{2+}$ entry phase across the plasma membrane, which is mediated through the SOCE pathway. As expected from the established pharmacological features of SOCE [22, 23], the compound 2-APB potentiated SOCE at 5 μM and inhibited at 50 μM (Figure 2A and S2B), demonstrating that LN229 cells bear the typical pharmacological signature of SOCE mediated through Orai1 channels. Leak control recordings in LN229 cells were performed in the absence of store depletion and showed insignificant $Ca^{2+}$ entry upon restoration of 2 mM $Ca^{2+}$ to the bath solution (Figure S2C). These results indicated that SOCE is functional in LN229 cells.

To investigate whether amlodipine either causes $Ca^{2+}$ release from ER stores or activates $Ca^{2+}$ entry across the plasma membrane in LN229 cells, we added 20 μM amlodipine in the absence of external $Ca^{2+}$ for several minutes followed by restoration of 2 mM $Ca^{2+}$ to the external milieu. In the absence of extracellular $Ca^{2+}$, amlodipine did not activate a $Ca^{2+}$ signal, suggesting that amlodipine does not cause $Ca^{2+}$ release from intracellular stores (Figure 2B, 2D-F). However, when extracellular $Ca^{2+}$ was replenished, amlodipine consistently activated a significant and sustained $Ca^{2+}$ signal in all cells (Figure 2B, 2D-F), suggesting that amlodipine activates a $Ca^{2+}$ entry route across the plasma membrane. To pharmacologically characterize the amlodipine-activated $Ca^{2+}$ entry pathway, we tested the effects of the drug 2-APB on this pathway. Similar to SOCE activated by thapsigargin and ionomycin, amlodipine-activated $Ca^{2+}$ entry was potentiated by 5 μM 2-APB and inhibited by 50 μM 2-APB, suggesting that amlodipine activated $Ca^{2+}$ entry through the SOCE channel Orai1 (Figure 2D). When used at relatively low concentrations (1–5 μM), the lanthanide ion $Gd^{3+}$ is a specific inhibitor of SOCE through Orai channel isoforms [22, 24, 25]. Consistently, $Gd^{3+}$ at 5 μM inhibited amlodipine-activated $Ca^{2+}$ entry (Figure 2E). ML-9 (50 μM) was reported to inhibit SOCE through a store-independent mechanism by causing rapid reversal of STIM1 aggregation [26], a process that is required for activation of SOCE through Orai1 channels. Interestingly, 50 μM ML-9 was unable to inhibit amlodipine-activated $Ca^{2+}$ entry (Figure 2F), further supporting that the effect of amlodipine on Orai1 channels is independent of store depletion and of STIM1 aggregation. We also examined the effects of amlodipine in normal human astrocytes (NHA). Although amlodipine can activate $Ca^{2+}$ entry in NHA, the magnitude of this $Ca^{2+}$ entry is significantly smaller than in LN229 cells (Figure 2G, 2H, S2D and S2E). This is consistent with the findings that SOCE in response to passive store depletion by thapsigargin is much smaller in NHA (Figure S2F) compared to LN229 (Figure S2I; blue trace), as reported previously [29]. To further examine the role of Orai1 channels in mediating the effect of amlodipine, we silenced the expression of Orai1, the pore forming subunit of SOCE channels, by using siRNA in LN229 cells (Figure S2G). As expected, knockdown of Orai1 significantly reduced SOCE in response to thapsigargin (Figure S2H; Figure S2I shows leak controls) as well as $Ca^{2+}$ entry in response to amlodipine treatment (Figure 2I and 2H). Collectively, these results show that SOCE is more robust in LN229 compared to NHA cells and that amlodipine activates $Ca^{2+}$ entry through Orai1 channel-mediated SOCE in LN229 cells.

In the absence of extracellular $Ca^{2+}$, 20 μM amlodipine caused an increase in emitted Fura2 fluorescence after excitation at both 340 nm and 380 nm (Figure S2J). Unlike the opposite effect on F340 (increase) and F380 (decrease) observed upon $Ca^{2+}$ binding to Fura2, this simultaneous increase in both F340 and F380 which translates into a decrease of F340/F380 ratio suggested that amlodipine emits green fluorescence upon excitation in the UV range, thus blunting the fura-2 signal. Indeed, addition of 20 μM amlodipine to HEK293 cells prior to activation of SOCE with 1 μM thapsigargin caused a significant decrease in fura-2 fluorescence signal throughout the recording (Fig. S2K, red trace) as previously described [30]. Significantly, washout of amlodipine restored the fura-2 signal in response to 1 μM thapsigargin to control levels without amlodipine (Figure S2K) strongly suggesting that amlodipine blunts the fura-2 signal and thus leads to underestimation of the overall intracellular $Ca^{2+}$ concentrations. Indeed, we show a robust $Ca^{2+}$ signal activated by

amlodipine when using the single excitation-single emission $Ca^{2+}$ dye Fluo4, which is excited in the blue range (Figure S2A), further ruling out potential non-specific effects of amlodipine. Taken together, these data suggest that amlodipine activates $Ca^{2+}$ entry through SOCE mediated by Orai1 channels. Amlodipine activates Orai1-mediated $Ca^{2+}$ entry independently of depletion of ER $Ca^{2+}$ stores.

### Activation of SOCE inhibits YAP/TAZ activities through the Hippo pathway

The above results suggested that SOCE-mediated cytosolic $Ca^{2+}$ elevation triggers YAP/TAZ phosphorylation. To test this notion, we used two specific SOCE activators, thapsigargin (1 μM) and ionomycin (1 μM), to trigger SOCE and increase intracellular $Ca^{2+}$. We found that ionomycin and thapsigargin can each robustly induce YAP/TAZ phosphorylation and the cytoplasmic translocation of YAP/TAZ in LN229 cells (Figure 3A and S3A). Correspondingly, we saw the up shift of TAZ protein bands in SDS-PAGE (Figure 3A), a typical phenomenon indicating protein phosphorylation. Therefore, we used this phenomenon as an indication of TAZ phosphorylation in the following studies.

To further investigate whether these effects are cytosolic $Ca^{2+}$-dependent, we used the cytosolic $Ca^{2+}$ chelator EGTA-AM. We found that adding EGTA-AM suppresses the effects of amlodipine on YAP/TAZ phosphorylation as well as cytoplasmic translocation (Figure 3B and3C upper panel). Similarly, the effect of ionomycin on YAP/TAZ cytoplasmic translocation was also compromised by EGTA-AM (Figure 3C lower panel). We then used a $Ca^{2+}$-free medium and found that under this condition, neither ionomycin nor thapsigargin induced YAP/TAZ phosphorylation and their cytoplasmic translocation (Figure 3D and3E). On the other hand, reintroduction of $Ca^{2+}$ into the medium restored the effects for ionomycin and thapsigargin, suggesting a crucial role for $Ca^{2+}$ entry from the external space. When similar $Ca^{2+}$-free medium was used to examine the effect of amlodipine, we found that amlodipine can still induce YAP phosphorylation to some extent (Figure 3D). We reasoned that a residual amount of $Ca^{2+}$ in the nominally $Ca^{2+}$ free medium or on the cell membranes might contribute amlodipine's effects. To test this, we added a very low concentration of EGTA, 25 μM into the $Ca^{2+}$-free medium and found that in this condition the induction of YAP phosphorylation by amlodipine was largely blocked (Figure S3D). Based on these results, we concluded that elevation of cytosolic $Ca^{2+}$ through SOCE induces YAP/TAZ phosphorylation and their translocation into the cytosol.

YAP/TAZ phosphorylation indicates activation of their kinases, Lats1/2. Indeed, we found that Lats1 phosphorylation on threonine 1079 (T1079), an essential step for Lats1 activation [31], was robustly induced by amlodipine, ionomycin or thapsigargin in LN229 cells (Figure 3A). We also found that the comparable threonine (T1041) in Lats2, which is the homology of Lats1, was also phosphorylated under the treatments of ionomycin or thapsigargin (Figure S3B). In the hippo pathway, MST1/2 are major kinases in charge of the phosphorylation of Lats1/2, although several other kinases were recently identified to have similar functions [32, 33]. We found that both ionomycin and thapsigargin induce MST1/2 phosphorylation (Figure 3A), suggesting their activation. To test if the effects of SOCE on the Hippo pathway are limited to LN229 cells, we examined several other GBM cell lines, including LN18 and DBTRG-05MG cells. In these cells, treatment by amlodipine, ionomycin or thapsigargin can

also robustly induce Lats1 and YAP phosphorylation, as well as YAP/TAZ cytoplasmic translocation (Figure S3C and data not shown). Interestingly, when examining NHA, we found that thapsigargin can only slightly induce TAZ phosphorylation but not phosphorylation of Lats1 and YAP (Figure S3E) compared to LN229 cells (Figure 3A). This is consistent with the observation that SOCE induced by thapsigargin in NHA is much weaker than LN229 cells (Figure S2I vs. S2F, blue trace). However, we found that amlodipine can still induce Lats1 and YAP/TAZ phosphorylation (Figure S3E). Given SOCE induced by amlodipine in NHA is also weaker than in LN229 cells (Figure 2I and2J), the effects on the Hippo pathway might be SOCE independent.

In our subsequent studies, we focused on using Lats1 and YAP phosphorylation as readout in LN229 cells to examine the mechanisms involved. Our experiments indicated that the effect of amlodipine, ionomycin or thapsigargin on Lats1 phosphorylation also depends on increased intracellular $Ca^{2+}$ through $Ca^{2+}$ entry from the extracellular space (Figure 3B, 3D and S3D). These results suggested that elevation of cytosolic $Ca^{2+}$ inhibits YAP/TAZ by activating Lats1. To further establish this connection, we knocked down Lats1 with a pool of siRNAs, and found that ionomycin-induced YAP/TAZ phosphorylation was not affected (Figure S3F). However, when both Lats1 and Lats2 were depleted by siRNAs, amlodipine- or ionomycin-induced YAP/TAZ phosphorylation was inhibited (Figure 3F). These results suggested that Lats1 and Lats2 are both involved in mediating YAP/TAZ phosphorylation. In agreement with this, depletion of Lats2 alone had no effect on ionomycin-induced YAP/TAZ phosphorylation, either (Figure S3F). Moreover, YAP/TAZ cytoplasmic translocation induced by amlodipine, ionomycin or thapsigargin also requires Lats1 and 2 (Figure S3G). We further found that depletion of both MST1 and MST2 inhibits amlodipine- and ionomycin-induced phosphorylation of Lats1, YAP and TAZ, as well as amlodipine-, ionomycin- or thapsigargin-induced YAP/TAZ cytoplasmic translocation (Figure 3F and S3G). Notably, TAZ protein levels appear to be still reduced by amlodipine or ionomycin in Lats1/2- or MST1/2-depleted cells. This might be due to other mechanisms independent on the core kinase cascade. Nevertheless, these results indicated that activating the MST1/2-Lats1/2 kinase cascade is a major mechanism to inhibit YAP/TAZ by elevation of cytosolic $Ca^{2+}$.

## $Ca^{2+}$-induced Lats1 activation and YAP/TAZ inhibition depends on cPKCs

Calcium is an intracellular messenger, which binds to multiple effectors and regulates downstream signaling. Among these effectors, conventional PKCs (cPKCs) were found to be involved in the Hippo pathway regulation by 12-O-Tetradecanoylphorbol-13-acetate (TPA, also known as PMA) and G-protein-coupled receptors (GPCRs) [34]. We examined the role of cPKCs by using a cPKCs specific inhibitor GO6976 [35]. We found that GO6976 blocked amlodipine- or ionomycin-induced Lats1 and YAP phosphorylation (Figure 4A), as well as YAP/TAZ cytoplasmic translocation in LN229 cells (Figure 4B). This inhibition was dose-dependent, with partial effect at as low as 0.25 μM and full inhibition at 1 μM (Figure S4A-C). These results supported that the inhibition by GO6976 is unlikely an off-target effect. We also observed similar inhibitory effects of GO6976 (1 μM) in LN18 and DBTRG-05MG cells (data not shown). These results suggested that cPKCs act downstream of $Ca^{2+}$ to activate Lats1/2.

There are four cPKC isoenzymes (alpha, beta I, beta II, and gamma). To investigate whether one particular isoenzyme could be the major mediator in $Ca^{2+}$ regulation of YAP/TAZ, we transiently expressed a dominant negative (DN) mutant of each isoenzyme [36] in LN229 cells (Figure 4C). Interestingly, we found that the beta II DN mutant is the most effective one in suppressing amlodipine-induced YAP/TAZ cytoplasmic translocation (Figure 4D and4E), while these DN mutants have no effects on YAP/TAZ localization in DMSO-treated cells (Figure S4D). We obtained similar results when examining ionomycin-induced YAP/TAZ cytoplasmic translocation (data not shown). These results suggested that PKC beta II is a major mediator of $Ca^{2+}$-induced YAP/TAZ inhibition in LN229 cells. To examine this notion, we employed a pool of siRNAs to knockdown PKC beta II (Figure S4E) and found that PKC beta II depletion suppressed thapsigargin- and amlodipine-induced phosphorylation of Lats1 and YAP (Figure 4F). To further investigate if PKC beta II mediates $Ca^{2+}$-induced Hippo pathway activation, we transiently expressed PKC beta II in LN229 cells and found that it enhanced amlodipine- and ionomycin-induced Lats1 and YAP phosphorylation (Figure 4G and4H). These results indicated that PKC beta II is a major mediator of $Ca^{2+}$-induced Lats1/2 activation.

Interestingly, we observed a mild induction of YAP phosphorylation by PKC beta II without the treatment of amlodipine or ionomycin (Figure 4G and H). In these experiments, we also examined the localization of YAP/TAZ and did not observe markedly difference between vector- and PKC beta II-transfected cells (data not shown). It was probably due to the technical limitation of imaging YAP/TAZ localization, which cannot detect the small difference as being showed by western blotting. Nevertheless, these results suggested that PKC beta II needs to be activated to trigger the robust effects on the Hippo pathway. Since PMA is a potent activator of cPKCs as well as novel PKCs (nPKCs), we examined whether activation of cPKCs by PMA can also activate Lats1/2 and inhibit YAP/TAZ. Interestingly, in contrast to ionomycin and thapsigargin, PMA (100 nM) treatment does not affect phosphorylation of Lats1, YAP or TAZ (Figure S4F), nor does it affect cytoplasmic-nuclear distribution of YAP/TAZ in LN229 cells (Figure S4G). To examine whether PMA in our experiments is an active compound, we used PKC beta II localization as readout. It was reported previously that PMA can induce PKC beta II to associate with the actin cytoskeleton[37]. We observed a similar effect in LN229 cells treated by PMA (100 nM) (Figure 5E). This result suggested that PMA is active. Overall, the above results suggested that PKC beta II is required but not sufficient to fully induce the Hippo pathway and YAP/TAZ phosphorylation. Additional effectors associating with $Ca^{2+}$ signals are likely required for this process.

## INF2-mediated CaAR is required for $Ca^{2+}$-induced Hippo pathway activation

To explore additional effectors in $Ca^{2+}$ activation of the Hippo pathway, we compared cell morphologies under different treatments. When treated by amlodipine, ionomycin, or thapsigargin, the periphery of LN229 cells retracts and these cells appeared to detach from the culture dishes (Figure 5A). The retraction and detachment can be blocked by co-treatment with GO6976 (Figure 5A), suggesting that cPKCs are responsible for these morphological changes. In contrast, PMA treatment induces these cells to flatten without detachment for up to 2 hours (Figure S5A and data not shown). Given it has been shown that

cell detachment activates the Hippo pathway [38], we focused on those cells in which amlodipine or ionomycin treatment produced no apparent morphological changes, hoping to answer whether cell detachment associated with amlodipine or ionomycin treatment is necessary for inducing YAP/TAZ cytoplasmic translocation. Interestingly, we found that these cells nevertheless showed significant amount of YAP/TAZ cytoplasmic translocation (Figure S5B). These results suggested that YAP/TAZ cytoplasmic translocation occurs before cell detachment. Notably, this assay does not rule out the possibility that early stages of cell periphery retraction are required for the YAP/TAZ regulation.

F-actin remodeling has been found to regulate the Hippo pathway although the mechanism remains unclear [39]. Our observations of changes in cell morphology induced by amlodipine, ionomycin, or thapsigargin implied actin cytoskeletal reorganization. It has been reported recently that calcium can induce actin filaments to assemble at the perinuclear rim and endoplasmic reticulum (ER) [40, 41]. The actin-filament assembly is accompanied by cortical actin-filament disassembly. Such actin remodeling was called calcium-mediated actin reset (CaAR). We performed time lapse imaging of F-actin labeled by EGFP-Lifeact [42] and found that ionomycin and thapsigargin can induce the assembly of actin filaments at the perinuclear rim (Figure 5B and S5C, arrows). These observations suggested that CaAR also occurs in LN229 cells. It has been previously shown that CaAR in 3T3 fibroblasts and Hela cells depends on a formin family protein, inverted formin-2 (INF2) [40, 41]. To examine whether CaAR was responsible for the Hippo pathway regulation by $Ca^{2+}$, we used siRNAs to silence the expression of INF2 in LN229 cells. We found that knockdown of INF2 effectively blocks the perinuclear assembly of actin filaments induced by ionomycin or thapsigargin (Figure 5B and S5C, arrowheads), suggesting that INF2 is also essential for CaAR in these cells. Under this circumstance, we examined the Hippo pathway and found that amlodipine, ionomycin or thapsigargin treatment was unable to induce the phosphorylation of Lats1 and YAP as effectively as in control cells (Figure 5C). These results indicated that INF2-mediated CaAR is essential for the Hippo pathway activation by $Ca^{2+}$.

## INF2-mediated CaAR is required for PKC beta II association with the actin cytoskeleton

Our results above have revealed that two factors, cPKCs and CaAR, are involved in the Hippo pathway activation by $Ca^{2+}$. Next, we sought to dissect their possible causal relations. Since cPKCs are required for the aforementioned cell morphological changes and the Hippo pathway activation, we investigated whether cPKCs were also involved in CaAR. We found that the perinuclear assembly of actin filaments induced by ionomycin or thapsigargin was not affected by the cPKCs inhibitor GO6976 (Figure 5D and S5D, arrows). These results suggested that cPKCs were not required for the actin filament assembly. On the other hand, given that PKC beta II is a major cPKC involved in the Hippo pathway activation by $Ca^{2+}$, we investigated whether CaAR affects the PKC beta II activity. It has been shown that PKC beta II is activated by binding to F-actin [37], therefore, we reasoned that CaAR may induce the interaction between PKC beta II and F-actin. Indeed, we found an enrichment of HA-tagged PKC beta II in the Triton-X100 insoluble actin cytoskeletal compartment after the treatment of ionomycin or thapsigargin (Figure 5E). Interestingly, knockdown of INF2 eliminates PKC beta II from this actin compartment (Figure 5E). Because the role of INF2

in CaAR is to mediate the actin remodeling [40, 41], this result suggested that INF2-mediated actin remodeling is required for the PKC beta II translocation to the cytoskeleton. Notably, PMA can also robustly induce PKC beta II translocation to an actin cytoskeletal compartment in this assay [37]. However, this translocation does not appear to depend on INF2 (Figure 5E). In addition, PMA treatment cannot induce the perinuclear assembly of actin filaments (Figure S5E). These differential dependencies on INF2 by PKC beta II translocations in response to $Ca^{2+}$ and PMA may explain why $Ca^{2+}$, but not PMA, activates the Hippo pathway. Collectively, these results suggested that INF2-mediated CaAR induces translocation of PKC beta II to certain actin compartments and activate the Hippo pathway.

## PKC Beta II suppresses GBM growth by inhibiting YAP/TAZ

To study whether cPKCs mediate $Ca^{2+}$ inhibition of YAP/TAZ activities, we examined the transcription of CTGF and Cyr61. Ionomycin treatment downregulates the transcription of these genes in LN229 cells. However, such inhibition was abolished when the cells were co-treated by the cPKC inhibitor, GO6976 (Figure 6A). Additionally, we found that cells stably expressing recombinant PKC beta II showed reduced expression of CTGF and Cyr61. In contrast, if the cells also express the $TAZ^{4SA}$ constitutively active mutant, PKC beta II cannot inhibit CTGF and Cyr61 expressions (Figure 6B). We also examined $YAP^{5SA}$ constitutively active mutant and found that its expression is able to antagonize the effect of PKC beta II on Cyr61 expression (Figure S6A). Interestingly, $YAP^{5SA}$ by itself reduces CTGF expression in this condition. This is probably due to a perturbation of other machineries required for CTGF expression. Nevertheless, under this circumstance, co-expression of PKC beta II showed no further inhibition of CTGF expression (Figure S6A). This result is also consistent with the notion that PKC beta II cannot inhibit CTGF expression in the presence of $YAP^{5SA}$. These results supported the notion that PKC beta II inhibits YAP/TAZ transcriptional activities by activating the Hippo pathway.

Since TAZ is required for LN229 cell growth and tumorigenesis (Figure S1A-F), we examined whether inhibiting TAZ with PKC beta II suppressed oncogenic properties of LN229 cells. We first performed a 2-D colony formation assay and found that LN229 cells that stably expressed PKC beta II exhibited reduced clonogenicity (Figure 6C). However, PKC beta II expression in $TAZ^{4SA}$- or $YAP^{5SA}$-transduced cells does not inhibit their colony-forming abilities (Figure 6C and S6B). To further examine the effects of PKC beta II on oncogenic properties, we conducted a 3-D tumorsphere assay, which reflects the stemness of tumor cells. We found that expression of PKC beta II inhibited tumorsphere formation by these cells, and co-expression of $TAZ^{4SA}$ or $YAP^{5SA}$ active mutant abolishes this inhibition (Figure 6D and S6C). These results suggested that PKC beta II is able to suppress the oncogenic properties of GBM cells by inhibiting YAP/TAZ activities, and that PKC beta II may have a tumor suppressor function in GBM. To test this notion, we employed the orthotopic mouse GBM model and found that PKC beta II expression in LN229 cells significantly reduced tumor growth in the brain (Figure 6E, upper panel and 6F). However, when co-expressing with $TAZ^{4SA}$ or $YAP^{5SA}$ in LN229 cells, PKC beta II cannot inhibit the tumor growth (Figure 6E, lower panel, 6F and S6D). In addition, mice with those tumors derived from PKC beta II-transduced LN229 cells survived longer than those from vector-transduced cells (Figure 6G). However, this difference was eliminated

when cells also expressed TAZ$^{4SA}$ or YAP$^{5SA}$ (Figure 6G and S6E). Therefore, our results above indicated that PKC beta II is able to inhibit GBM growth and prolong mouse survival by inhibiting YAP/TAZ.

## Discussion

In this study, we uncovered a way to inhibit YAP/TAZ in GBM by activating Lats1/2 kinases (Figure 7). Elevation of cytosolic Ca$^{2+}$ by triggering SOCE induces phosphorylation and activation of Lats1/2. We then identified that PKC beta II is a major mediator for Ca$^{2+}$-induced Lats1/2 phosphorylation. Ca$^{2+}$ induces PKC beta II to accumulate in an actin cytoskeletal compartment. Such PKC beta II translocation depends on INF2. Depletion of INF2 by siRNAs disrupts both Ca$^{2+}$-induced PKC beta II translocation to the actin cytoskeleton and Ca$^{2+}$-induced Lats1/2 activation. Furthermore, we showed that elevation of cytosolic Ca$^{2+}$ or PKC beta II expression inhibits YAP/TAZ-mediated gene transcription and that PKC beta II expression inhibits glioblastoma cell growth, stemness and tumorigenesis by inhibiting YAP/TAZ. Collectively, these findings suggested that Ca$^{2+}$-induced F-actin remodeling provides a scaffold for PKC beta II to activate the Hippo pathway and inhibit YAP/TAZ.

In human primary GBM cells, knockdown of STIM1 or Orai1 inhibited cell invasion [29]. Blocking Orai1 channels pharmacologically or by RNAi in the rat glioblastoma cell line C6 attenuated cell proliferation and induced apoptosis [43]. These early studies suggested that SOCE contributes to GBM cell migration, proliferation and survival. Our results here showed that pharmacological activation of SOCE channels can inhibit cell survival. This suggests that while SOCE provides a growth advantage to GBM cells under resting conditions, robust pharmacological activation of SOCE can inhibit survival through Ca$^{2+}$ overload-induced YAP/TAZ inhibition. Given a higher level of SOCE exists in GBM cells than normal astrocytes [29], Ca$^{2+}$ overload might be easier to achieve in tumor cells. This may provide a potential intervention window for therapeutic purposes. Notably, our results indicated that the concentrations of amlodipine to activate Orai1 channels and inhibit cell survival are around 10 μM, which is much higher than the maximum steady state plasma concentration (~ 0.04 μM) in clinical studies for its original usage as a hypertension drug [44]. Therefore, finding a way to effectively activate SOCE in tumor cells is needed in the future.

The role of PKC in regulating the Hippo pathway has been previously studied [34]. It was found that PMA induces YAP/TAZ dephosphorylation or phosphorylation depending on differential cellular contexts. In HEK293A cells, PMA induces YAP/TAZ dephosphorylation, and cPKCs promote this effect. Our studies also identified a role of cPKCs in Hippo pathway regulation. However, the Ca$^{2+}$-induced Hippo pathway regulation appears to be different from the previously reported PMA-induced regulation. First, our results indicated that cPKCs promote YAP/TAZ phosphorylation. Second, we found that PMA treatment cannot induce YAP/TAZ phosphorylation as effectively as ionomycin and thapsigargin do in the same cells. Third, our studies suggested that MST1/2 are essential for Ca$^{2+}$-induced regulations of Lats1/2 and YAP/TAZ. Furthermore, we found that unlike Ca$^{2+}$, PMA cannot induce CaAR-like actin remodeling. This difference in CaAR induction may determine the differential effects of Ca$^{2+}$ and PMA on the Hippo pathway.

Our studies revealed that the dominant negative PKC beta II mutant effectively suppresses the cytoplasmic translocation of YAP/TAZ, whereas the dominant negative mutants of other cPKC isoforms have little or no effects. The differential effects among these mutants may reflect the different extents of involvement by individual cPKCs in $Ca^{2+}$-induced Hippo pathway activation. One possibility is due to differences in expression levels of these cPKCs. Our qPCR analyses indicated that the expression of the PKC beta I isoform is about 30-fold lower than PKC beta II isoform in LN229 cells (data not shown). However, the expression of PKC alpha is readily detected in these cells. Therefore, the involvement of individual cPKC isoenzymes in $Ca^{2+}$-induced Hippo pathway activation cannot be explained solely by the differences in their expression. Our studies found a $Ca^{2+}$-induced accumulation of PKC beta II in an actin cytoskeletal compartment. Notably, PKC beta II is the only PKC that contains a F-actin binding motif at its V5 carboxyl terminus and can be activated by F-actin [37, 45]. Therefore, it is likely that $Ca^{2+}$-induced actin cytoskeleton remodeling provides a scaffold for PKC beta II to regulate the Hippo pathway.

The actin cytoskeleton is an important component in transducing upstream signals to YAP/TAZ in Lats1/2-dependent and -independent manners [39, 46]. It has been proposed that stress fibbers or other unknown cell spreading associated F-actin networks serve as platforms to regulate certain Hippo pathway regulators [39]. Consistently, Angiomotin, which is a direct inhibitor of YAP/TAZ, was found to be sequestered by F-actin [47]. However, how Lats1/2 are regulated by F-actin was unknown. Here, our studies suggested a different perspective by which how actin cytoskeleton regulates the Hippo pathway. Instead of simple disruption of F-actin, assembly of new actin filaments may actively regulate the Hippo pathway. Therefore, in addition to sequestering a YAP/TAZ inhibitory factor, such as Angiomotin [47], by the old F-actin [39], the newly-formed actin filaments may provide a scaffold to launch Lats1/2 activators, such as PKC beta II. Although MST1/2 are still important for Lat1/2 phosphorylation, it remains to be determined if PKC beta II activates Lats1/2 by direct phosphorylation or indirect mechanisms. CaAR occurs in response to a variety of physiological cues, such as G-protein-coupled receptors activation and mechanical stimulation [40, 41], it would be interesting to examine whether similar regulation of the Hippo pathway by CaAR also exists in other Hippo pathway regulatory circumstances.

Taken together, our results indicate that $Ca^{2+}$ is an intracellular cue in activating the Hippo pathway and inhibiting YAP/TAZ. The regulation occurs through $Ca^{2+}$-mediated actin reset and depends on INF2 and PKC beta II. In this process, $Ca^{2+}$-induced F-actin re-assembly may provide a scaffold for PKC beta II to induce Lats1/2 phosphorylation by MST1/2. In addition, we found that amldodipine activates $Ca^{2+}$ entry through an Orai channel isoform in a store-independent manner. This provides a way to elevate cytosolic $Ca^{2+}$ thereby inhibiting YAP/TAZ in tumor cells. Our findings provide a novel perspective on how the Hippo pathway is regulated by the actin cytoskeleton and suggest robust SOCE activation as a strategy to suppress YAP/TAZ signaling in GBM as well as other cancers.

## Material & Methods

### Mice

Six to eight-week-old female nude mice (Nu(NCr)-Foxn1nu, from Charles River, Strain Code: 490) were used in the studies. For tumorigenesis experiments, LN229 cells were firstly transduced in vitro with a retrovirus vector expressing firefly luciferase. These cells were then transduced in vitro with retrovirus or lentivirus vectors expressing indicated shRNAs or cDNAs. $3\times10^5$ cells were injected intracranially. Bioluminescence imaging (BLI) was used to monitor tumor growth in brains. Briefly, mice were anesthetized with isoflurane. 1.875 mg of luciferin dissolved in 125 μL of PBS (15 mg/ml) was i.p. injected into mice. Ten minutes later, the mice were placed in the IVIS imaging chamber (Xenogen, Alameda, CA) and imaged for 1 min with the camera set at the highest sensitivity. Photons emitted from the brain region were quantified using LivingImage software (Xenogen). Luciferase activity was presented as the photons emitted/s. All experiments were performed in accordance with the Penn State University Institutional Animal Care and Use Committee guidelines.

### Cells

LN229 (CRL-2611), LN18 (CRL-2610), T98G (CRL-1690) and DBTRG-05MG (CRL-2020) human glioblastoma cell lines were from ATCC. Normal Human Astrocytes (NHA, CC-2565) were from LONZA. LN229, LN18, T98G and DBTRG-05MG cells were cultured in Dulbecco's modified Eagle's medium (DMEM) (Corning, 10–013-CV) supplemented with 10% Fetal Bovine Serum (Gibco, 10437028) and 1% Antibiotic-Antimycotic Solution (Corning, 30–004-CI) at 37°C with 5% $CO_2$. NHA were cultured in NHA growth medium according to the standard protocol as described in the instructions for the Human Astrocyte Cell System (LONZA). None of these cell lines were listed in the database of misidentified cell lines maintained by ICLAC and NCBI Biosample. These cell lines were not authenticated in this study. All cell lines were examined to be mycoplasma negative before experiments.

Unless otherwise indicated, experiments were performed with cells grown to 50% confluency. For compound treatment experiments, cells were seeded in complete medium (10% FBS) for overnight and treated with DMEM medium containing 2% FBS and indicated compounds for indicated times before harvest. For NHA, the NHA growth medium was used in the treatment. For calcium-dependent experiments, after overnight culture in complete medium, cells were pre-incubated in calcium free medium (Invitrogen, #21068028) supplemented with 2mM Glutamine and 2% FBS for 1 hour. Calcium free or calcium-containing DMEM (containing 2mM $CaCl_2$) with indicated compounds was then added to cells. For compound combination experiments, cells were preincubated with GO6976 or EGTA-AM for 1 hour before indicated compound mixture were added to cells.

### Antibodies and Compounds

Anti-Phospho-LATS1 (Thr1079) (8654), anti-Phospho-MST1 (Thr183)/MST2 (Thr180) (3681), anti-Phospho-YAP (Ser127) (13008), anti-Phospho-TAZ (Ser89) (59971), anti-YAP (12395), anti-TAZ (4883), anti-Lats1 (3477), anti-Lats2 (5888), anti-MST1 (14946), anti-

MST2 (3952), anti-YAP/TAZ (8418) (an antibody recognizing both YAP and TAZ) and anti-alpha-tubulin (3873) antibodies were from Cell Signaling Technology. Anti-INF2 (ABT-61) antibody was from Millipore. Anti-HA (MMS-101P) antibody was from BioLegend. Anti-β-Actin (A5316) and anti-Orai1(O8264) antibodies were from Sigma-Aldrich. Goat anti-mouse IgG-HRP (sc-2005), goat anti-rabbit IgG-HRP (sc-2004) antibodies were from Santa Cruz Biotechnology. Anti-alpha-tubulin (12G10) was from Developmental Studies Hybridoma Bank. Amlodipine (S1905), Amlodipine besylate (S1813), GO6976 (S7119) were from Selleck Chemicals. Ionomycin (I9657), Thapsigargin (586005) and Phorbol 12-myristate 13-acetatewere (PMA) (P1585) were from Sigma-Aldrich. EGTA-AM (324628) was from Calbiochem.

## Vectors

pBabe-neo-TAZ (4SA), pBabe-neo-YAP (5SA) were described previously [20, 21] and generously provided by Kun-Liang Guan. pHACE-PKC alpha DN (21235), pHACE-PKC beta I DN (16381), pHACE-PKC beta II DN (16385) and pHACE-PKC gamma DN (21239) were described preciously [36] and gifts from Bernard Weinstein via Addgene. mEGFP-Lifeact-7 (54610) was a gift from Michael Davidson via Addgene. To generate pHACE-PKC beta II wild-type, pHACE-PKC beta II DN (16385) was subjected to site-directed mutagenesis using the Quickchange mutagenesis Kit (Stratagene). To generate pBabe-puro-PKC beta II wild-type, HA-tagged PKC beta II wild-type from pHACE-PKC beta II wild-type was subcloned into the pBabe-puro vector.

## Small molecule screen

LN229 cells were seeded in 20 μl of DMEM containing 2% FBS per well into 384-well plates (Corning) using an automated plate filler (BioTek). After 24 hours, 10 μl of compound solution were transferred into the 384-well plates resulting in ~10 μM final drug concentration. Each plate also included DMSO only negative controls and staurosporine (2μM) positive control. After 72 hours incubation, cell viability was determined in each well using the PrestoBlue Cell Viability Reagent (Invitrogen) and read in a multi-mode plate reader (BMG Labtech). Luminescence data were normalized to DMSO as 100% viable and Staurosporine as 0% viable.

## Immunoblotting

Immunoblotting procedure was described previously [48]. Briefly, cells were lysed in SDS-lysis buffer (10 mM Tris pH 7.5, 1% SDS, 50 mM NaF, 1 mM NaVO$_4$) and subjected to SDS-PAGE on 4–12% Bis-Tris SDS-PAGE gels (Invitrogen) and transferred to Immobilon-P membranes (Millipore). Membranes were incubated in blocking buffer: 5% skim milk/TBST (0.1% Tween, 10 mM Tris at pH 7.6, 100 mM NaCl) for 1 hour at room temperature and then with primary antibodies diluted in 5% BSA/TBST overnight at 4°C. After three washes, the membranes were incubated with goat anti-rabbit HRP-conjugated antibody (1:5,000; Santa Cruz sc-2054) or goat anti-mouse HRP-conjugated antibody (1:10,000; Santa Cruz sc-2005) at room temperature for 2 hours and subjected to chemiluminescence using ECL (Pierce #1856136).

## Immunofluorescent Staining

Immunofluorescent staining was described previously [48]. Briefly, cells were fixed with 4% paraformaldehyde in PBS for 20 min and incubated in permeabilization buffer (PDT: 0.3% sodium deoxycholate, 0.3% Triton X-100 in PBS) for 30 min on ice. They were then blocked with 5% BSA/PBS at 4°C for 1hr and followed by incubating overnight at 4°C with primary antibodies diluted in 2.5% BSA/0.05% Triton X-100/PBS. After washing with 0.1% Triton X-100/PBS, cells were incubated with secondary antibodies diluted in 2.5% BSA/ 0.05% Triton X-100/PBS for 2 hours at 4°C. Cells were washed with 0.1% Triton X-100/ PBS, rinsed with PBS, and mounted in ProLong Gold Mountant (Invitrogen #P10144). When indicated, nuclei were stained with DAPI.

## Quantification of YAP/TAZ localization

The percentages of cells showing cytoplasmic YAP/TAZ signal more than or equal to nuclear YAP/TAZ signal were calculated. For inhibition index showing in Figure 4D, the above percentages were calculated for HA-positive cells (HA$^+$%) and HA-negative cells(HA$^-$%), respectively. Inhibition index = 1- HA$^+$%/ HA$^-$%.

## Subcellular Fractionation

Cytoskeleton fractionation was described previously [37]. Briefly, Cells were rinsed twice with ice cold PBS followed by adding 1% Triton X-100 solubilization buffer (15 mM Tris, pH 7.5, 120 mM NaCl, 25 mM KCl, 1% (v/v) Triton X-100, and 1X proteinase inhibitors). After incubation on dish at 4°C for 10 min, cells were harvested into a 1.5ml tube. Cell lysates were centrifuged at 21,000 g at 4°C for 40 min. The supernatant was saved as the soluble fraction (SUP). After washing with 1% Triton X-100 solubilization buffer, the pellet was suspended with SDS-lysis buffer (10 mM Tris pH 7.5, 1% SDS, 50 mM NaF, 1 mM NaVO$_4$) and assayed as the Triton insoluble fraction (CSK).

## Gene Expression and Silencing

Transient transfections were performed using Fugene 6 (Promega), Lipofectamine 2000 (Invitrogen) or DharmaFECT 1 (Dharmacon) by following the manufacturer recommended protocols. Retroviral generation and infection were described previously [48]. Lentiviral vectors encoding shRNAs targeting TAZ (#7: TRCN0000370007; #69: TRCN0000019469) were from Sigma-Aldrich. ON-TARGETplus SMARTpool siRNAs against Lats1, Lats2, MST1, MST2, PKC beta, INF2 or ON-TARGETplus siCONTROL were from Dharmacon. siRNA for Orai1 (sequence: CGUGCACAAUCUCAACUCGUU) was from Integrated DNA Technologies (IDT). For si-Orai1 control, AllStars Negative Control siRNA (SI03650318) was from Qiagen.

## Quantitative RT-PCR

qRT-PCR was carried out according to standard protocols. Briefly, total RNA was extracted using TRIzol reagent (Invitrogen). cDNAs were synthesized with iScript cDNA Synthesis kit (Bio-Rad, 1708891), and qPCR was carried out on a CFX96 Touch Real-Time PCR Detection System with SsoAdvanced Universal SYBR Green Supermix (Bio-Rad, 1725271). GAPDH was used as an internal reference to normalize the input cDNA. Primer sequences

used: PKC beta II forward, GACCAAACACCCAGGCAAAC, reverse, GATGGCGGGTGAAAAATCGG; CTGF forward, GCAGGCTAGAGAAGCAGAGC, reverse, ATGTCTTCATGCTGGTGCAG; Cyr61 forward, ACTTCATGGTCCCAGTGCTC, reverse, TGGTCTTGCTGCATTTCTTG; GAPDH forward, GGAGCGAGATCCCTCCAAAAT, reverse, GGCTGTTGTCATACTTCTCATGG.

The primers were designed using PrimerBank.

### Live cell imaging

Live cell microscopy was performed on *DeltaVision Elite* Inverted Microscope (Applied Precision Inc., WA) at 37°C and 5% $CO_2$ using 60X oil immerging objective. LN229 cells stably transduced by EGFP-Lifeact were plated on 35mm glass bottom microwell petri dishes (MatTek corporation, MA) at a density of $5 \times 10^5$ cells. Two hours prior to image acquisition, culture media was replaced with DMEM supplemented with 2% FBS. Throughout imaging acquisition, dishes were maintained in a sealed heated chamber so that temperature and $CO_2$ levels were both kept constant. Image fields were pre-selected with z sections spaced at 0.2 μm and total thickness of 4 μm (20 slices). Baseline conditions were recorded for 5 minutes, followed by treatment of either thapsigargin or ionomycin, both final concentration at 1 μM diluted in DEME with 2% FBS. Time-lapse images were acquired every minute with total recording time of 40 minutes. Final images were processed via deconvolution using the same working software.

### Calcium ($Ca^{2+}$) measurements

For intracellular $Ca^{2+}$ measurements using Fura-2, LN229 cells were cultured on 30-mm glass coverslips for 24 hours in complete media. Coverslips were then mounted in a Teflon chamber and incubated at 37°C for 30 min in complete culture medium with 2 μM fura-2 AM. Cells were then washed a total of 4 times with HEPES-buffered saline solution (140 mM NaCl, 1.13 mM $MgCl_2$, 4.7 mM KCl, 2 mM $CaCl_2$, 10mM D-glucose, and 10 mM HEPES; pH 7.4) and kept in this solution at room temperature for 10 min prior to $Ca^{2+}$ imaging. To record and analyze fura-2 fluorescence from LN229 cells, a digital fluorescence imaging system (InCyt Im2; Intracellular Imaging, Cincinnati, OH, USA) was used. Fura-2 was alternately excited at 340 and 380 nm and emitted fluorescence was collected at 510 nm. For each pixel, the emission ratio of 340/380-nm was represented. The addition of amlodipine causes an equal increase of emitted fluorescence upon excitation at both the 340 and 380 nm, suggesting that amlodipine emits fluorescence upon UV excitation. This amlodipine fluorescence was subtracted from the overall recordings. Amlodipine fluorescence masks the fura-2 signal in a dose dependent manner and leads to underestimation of the $Ca^{2+}$ signal activated by amlodipine. Solutions with thapsigargin, ionomycin, and amlodipine were suspended in HEPES-buffered saline solution. $Ca^{2+}$ traces are averages from many cells per coverslip and multiple independent experiments as indicated on respective figures. For intracellular $Ca^{2+}$ measurements using Fluo-4 NW, assay was carried out according to the manufacturer's protocols (Invitrogen, F36206). Briefly, cells were loaded with 2 μM Fluo-4 NW in the HEPES-buffered saline solution (HBSS) at 37 °C for 30 min. After 30min of incubation at 37 °C, calcium flux assays were performed with on-line compound addition in a FlexStation 3 plate reader (Molecular Devices), with

simultaneous data collection. Dose response curves were generated by SoftMaxPro (Molecular Devices).

### Colony formation assay

LN229 cells were trypsinized, resuspended and counted. 400 cells were seeded in complete culture medium per well of a 6-well plate and cultured for 10–12 days. The plates were then washed with PBS and stained with crystal violet. Colonies images were scanned and scored using Image J.

### Tumorsphere assay

LN229 cells were trypsinized, resuspended and counted. 500 cells were seeded in neural sphere medium (DMEM/F12, Corning #15–090-CV, L-glutamine, 2mM, Invitrogen #25030–081, N-2 supplement, 1X, Invitrogen #17502048, B-27 Supplement, 1X, Invitrogen #17504044, BSA, 50ug/ml, Sigma, EGF & bFGF, 20 ng/ml each, R&D systems, Antibiotic-Antimycotic Solution, 1% Corning #30–004-CI) containing 0.34% low melting temperature agarose (Invitrogen #18300012) per well in 24-well Ultra Low Cluster Plates (Costar). After solidification at 4°C for 5 minutes, the plates were incubated at 37°C for 2–3 weeks. Tumorspheres were stained by MTT (Invitrogen), scanned and scored using Image J.

### MTT cell viability assay

Cells were seeded in DMEM medium containing 2% FBS at a density of 3000 cells per well in 96-well plates. After overnight culture, cells were treated with indicated agents for 3 days. Viable cell numbers were determined using the MTT (3-(4,5-Dimethylthiazol-2-yl)-2,5-Diphenyltetrazolium Bromide) (Invitrogen #M6494) reagent according to the manufacturer's protocols (Invitrogen). Each assay consisted of two or three replicate wells. Data were presented as normalized to control cells (treated by DMSO).

### Statistical Methods

For statistical analyses (including animal studies), samples sizes were chosen based on if the differences between groups are biologically meaningful and are statistically significant. No data were excluded from the analyses. For cell experiments, all cells in one experiment were from the same pooled parental cells. All mice were from the same cohort. The mice were randomly picked to implant different types of cells. For data collection relying on objective instruments, such as plate reader, q-PCR, Microscopy software, animal IVIS system, and western blotting, the investigators were not blinded to group allocation during data collection. For animal studies, the investigators were not blinded to group allocation during data collection. The variance is similar between the groups that are being statistically compared. Statistical significance was determined by unpaired two-tailed student's t-test unless indicated otherwise. All center values shown were mean, and all error bars shown were standard error of the mean (s.e.m). All statistical calculations and plotting were performed using Graphpad Prism 7.

## Supplementary Material

Refer to Web version on PubMed Central for supplementary material.

## References

1. Ohgaki H, Kleihues P. Epidemiology and etiology of gliomas. Acta Neuropathol 2005; 109: 93–108. [PubMed: 15685439]

2. Phillips HS, Kharbanda S, Chen R, Forrest WF, Soriano RH, Wu TD et al. Molecular subclasses of high-grade glioma predict prognosis, delineate a pattern of disease progression, and resemble stages in neurogenesis. Cancer Cell 2006; 9: 157–173. [PubMed: 16530701]

3. Verhaak RG, Hoadley KA, Purdom E, Wang V, Qi Y, Wilkerson MD et al. Integrated genomic analysis identifies clinically relevant subtypes of glioblastoma characterized by abnormalities in PDGFRA, IDH1, EGFR, and NF1. Cancer Cell 2010; 17: 98–110. [PubMed: 20129251]

4. Bhat KP, Salazar KL, Balasubramaniyan V, Wani K, Heathcock L, Hollingsworth F et al. The transcriptional coactivator TAZ regulates mesenchymal differentiation in malignant glioma. Genes Dev 2011; 25: 2594–2609. [PubMed: 22190458]

5. Orr BA, Bai H, Odia Y, Jain D, Anders RA, Eberhart CG. Yes-associated protein 1 is widely expressed in human brain tumors and promotes glioblastoma growth. Journal of neuropathology and experimental neurology 2011; 70: 568–577. [PubMed: 21666501]

6. Yu FX, Zhao B, Guan KL. Hippo Pathway in Organ Size Control, Tissue Homeostasis, and Cancer. Cell 2015; 163: 811–828. [PubMed: 26544935]

7. Harvey KF, Zhang X, Thomas DM. The Hippo pathway and human cancer. Nat Rev Cancer 2013; 13: 246–257. [PubMed: 23467301]

8. Zanconato F, Cordenonsi M, Piccolo S. YAP/TAZ at the Roots of Cancer. Cancer Cell 2016; 29: 783–803. [PubMed: 27300434]

9. Tian T, Li A, Lu H, Luo R, Zhang M, Li Z. TAZ promotes temozolomide resistance by upregulating MCL-1 in human glioma cells. Biochem Biophys Res Commun 2015; 463: 638–643. [PubMed: 26043698]

10. Fernandez LA, Squatrito M, Northcott P, Awan A, Holland EC, Taylor MD et al. Oncogenic YAP promotes radioresistance and genomic instability in medulloblastoma through IGF2-mediated Akt activation. Oncogene 2012; 31: 1923–1937. [PubMed: 21874045]

11. Kapoor A, Yao W, Ying H, Hua S, Liewen A, Wang Q et al. Yap1 activation enables bypass of oncogenic Kras addiction in pancreatic cancer. Cell 2014; 158: 185–197. [PubMed: 24954535]

12. Shao DD, Xue W, Krall EB, Bhutkar A, Piccioni F, Wang X et al. KRAS and YAP1 converge to regulate EMT and tumor survival. Cell 2014; 158: 171–184. [PubMed: 24954536]

13. Johnson R, Halder G. The two faces of Hippo: targeting the Hippo pathway for regenerative medicine and cancer treatment. Nat Rev Drug Discov 2014; 13: 63–79. [PubMed: 24336504]

14. Monteith GR, Prevarskaya N, Roberts-Thomson SJ. The calcium-cancer signalling nexus. Nat Rev Cancer 2017; 17: 367–380. [PubMed: 28386091]

15. Roderick HL, Cook SJ. Ca2+ signalling checkpoints in cancer: remodelling Ca2+ for cancer cell proliferation and survival. Nat Rev Cancer 2008; 8: 361–375. [PubMed: 18432251]

16. Potier M, Trebak M. New developments in the signaling mechanisms of the store-operated calcium entry pathway. Pflügers Archiv : European journal of physiology 2008; 457: 405–415. [PubMed: 18536932]

17. Trebak M, Putney JW. ORAI Calcium Channels. Physiology 2017; 32: 332–342. [PubMed: 28615316]

18. Jardin I, Rosado JA. STIM and calcium channel complexes in cancer. Biochim Biophys Acta 2016; 1863: 1418–1426. [PubMed: 26455959]

19. Li W, Dong S, Wei W, Wang G, Zhang A, Pu P et al. The role of transcriptional coactivator TAZ in gliomas. Oncotarget 2016; 7: 82686–82699. [PubMed: 27764783]

20. Lei QY, Zhang H, Zhao B, Zha ZY, Bai F, Pei XH et al. TAZ promotes cell proliferation and epithelial-mesenchymal transition and is inhibited by the hippo pathway. Mol Cell Biol 2008; 28: 2426–2436. [PubMed: 18227151]

21. Zhao B, Wei X, Li W, Udan RS, Yang Q, Kim J et al. Inactivation of YAP oncoprotein by the Hippo pathway is involved in cell contact inhibition and tissue growth control. Genes Dev 2007; 21: 2747–2761. [PubMed: 17974916]

22. DeHaven WI, Smyth JT, Boyles RR, Bird GS, Putney JW. Complex actions of 2-aminoethyldiphenyl borate on store-operated calcium entry. Journal of Biological Chemistry 2008; 283: 19265–19273. [PubMed: 18487204]

23. Prakriya M, Lewis RS. Potentiation and inhibition of Ca2+ release-activated Ca2+ channels by 2-aminoethyldiphenyl borate (2-APB) occurs independently of IP3 receptors. Journal of Physiology 2001; 536: 3–19. [PubMed: 11579153]

24. Trebak M, Bird GSJ, McKay RR, Putney JW. Comparison of human TRPC3 channels in receptor-activated and store-operated modes. Differential sensitivity to channel blockers suggests fundamental differences in channel composition. Journal of Biological Chemistry 2002; 277: 21617–21623. [PubMed: 11943785]

25. Abdullaev IF, Bisaillon JM, Potier M, Gonzalez JC, Motiani RK, Trebak M. Stim1 and orai1 mediate crac currents and store-operated calcium entry important for endothelial cell proliferation. Circulation Research 2008; 103: 1289–1299. [PubMed: 18845811]

26. Smyth JT, DeHaven WI, Bird GS, Putney JW. Ca2+-store-dependent and -independent reversal of Stim1 localization and function. Journal of cell science 2008; 121: 762–772. [PubMed: 18285445]

27. Morgan AJ, Jacob R. Ionomycin enhances Ca2+ influx by stimulating store-regulated cation entry and not by a direct action at the plasma membrane. The Biochemical journal 1994; 300 ( Pt 3: 665–672. [PubMed: 8010948]

28. Takemura H, Hughes AR, Thastrup O, Putney JW. Activation of calcium entry by the tumor promoter thapsigargin in parotid acinar cells. Evidence that an intracellular calcium pool, and not an inositol phosphate, regulates calcium fluxes at the plasma membrane. Journal of Biological Chemistry 1989; 264: 12266–12271. [PubMed: 2663854]

29. Motiani RK, Hyzinski-Garcia MC, Zhang X, Henkel MM, Abdullaev IF, Kuo YH et al. STIM1 and Orai1 mediate CRAC channel activity and are essential for human glioblastoma invasion. Pflugers Arch 2013; 465: 1249–1260. [PubMed: 23515871]

30. Asai M, Takeuchi K, Uchida S, Urushida T, Katoh H, Satoh H et al. Misinterpretation of the effect of amlodipine on cytosolic calcium concentration with fura-2 fluorospectrometry. Naunyn-Schmiedeberg's Archives of Pharmacology 2008; 377: 423–427.

31. Chan EH, Nousiainen M, Chalamalasetty RB, Schafer A, Nigg EA, Sillje HH. The Ste20-like kinase Mst2 activates the human large tumor suppressor kinase Lats1. Oncogene 2005; 24: 2076–2086. [PubMed: 15688006]

32. Meng Z, Moroishi T, Mottier-Pavie V, Plouffe SW, Hansen CG, Hong AW et al. MAP4K family kinases act in parallel to MST1/2 to activate LATS1/2 in the Hippo pathway. Nat Commun 2015; 6: 8357. [PubMed: 26437443]

33. Zheng Y, Wang W, Liu B, Deng H, Uster E, Pan D. Identification of Happyhour/MAP4K as Alternative Hpo/Mst-like Kinases in the Hippo Kinase Cascade. Dev Cell 2015; 34: 642–655. [PubMed: 26364751]

34. Gong R, Hong AW, Plouffe SW, Zhao B, Liu G, Yu FX et al. Opposing roles of conventional and novel PKC isoforms in Hippo-YAP pathway regulation. Cell Res 2015; 25: 985–988. [PubMed: 26206313]

35. Martiny-Baron G, Kazanietz MG, Mischak H, Blumberg PM, Kochs G, Hug H et al. Selective inhibition of protein kinase C isozymes by the indolocarbazole Go 6976. J Biol Chem 1993; 268: 9194–9197. [PubMed: 8486620]

36. Soh JW, Weinstein IB. Roles of specific isoforms of protein kinase C in the transcriptional control of cyclin D1 and related genes. J Biol Chem 2003; 278: 34709–34716. [PubMed: 12794082]

37. Blobe GC, Stribling DS, Fabbro D, Stabel S, Hannun YA. Protein kinase C beta II specifically binds to and is activated by F-actin. J Biol Chem 1996; 271: 15823–15830. [PubMed: 8663149]

38. Zhao B, Li L, Wang L, Wang CY, Yu J, Guan KL. Cell detachment activates the Hippo pathway via cytoskeleton reorganization to induce anoikis. Genes Dev 2012; 26: 54–68. [PubMed: 22215811]

39. Halder G, Dupont S, Piccolo S. Transduction of mechanical and cytoskeletal cues by YAP and TAZ. Nat Rev Mol Cell Biol 2012; 13: 591–600. [PubMed: 22895435]

40. Shao X, Li Q, Mogilner A, Bershadsky AD, Shivashankar GV. Mechanical stimulation induces formin-dependent assembly of a perinuclear actin rim. Proc Natl Acad Sci U S A 2015; 112: E2595–2601. [PubMed: 25941386]

41. Wales P, Schuberth CE, Aufschnaiter R, Fels J, Garcia-Aguilar I, Janning A et al. Calcium-mediated actin reset (CaAR) mediates acute cell adaptations. Elife 2016; 5.

42. Riedl J, Crevenna AH, Kessenbrock K, Yu JH, Neukirchen D, Bista M et al. Lifeact: a versatile marker to visualize F-actin. Nat Methods 2008; 5: 605–607. [PubMed: 18536722]

43. Liu H, Hughes JD, Rollins S, Chen B, Perkins E. Calcium entry via ORAI1 regulates glioblastoma cell proliferation and apoptosis. Exp Mol Pathol 2011; 91: 753–760. [PubMed: 21945734]

44. Faulkner JK, McGibney D, Chasseaud LF, Perry JL, Taylor IW. The pharmacokinetics of amlodipine in healthy volunteers after single intravenous and oral doses and after 14 repeated oral doses given once daily. Br J Clin Pharmacol 1986; 22: 21–25. [PubMed: 2943308]

45. Steinberg SF. Structural basis of protein kinase C isoform function. Physiological reviews 2008; 88: 1341–1378. [PubMed: 18923184]

46. Sun S, Irvine KD. Cellular Organization and Cytoskeletal Regulation of the Hippo Signaling Network. Trends Cell Biol 2016; 26: 694–704. [PubMed: 27268910]

47. Mana-Capelli S, Paramasivam M, Dutta S, McCollum D. Angiomotins link F-actin architecture to Hippo pathway signaling. Mol Biol Cell 2014; 25: 1676–1685. [PubMed: 24648494]

48. Li W, Cooper J, Zhou L, Yang C, Erdjument-Bromage H, Zagzag D et al. Merlin/NF2 loss-driven tumorigenesis linked to CRL4(DCAF1)-mediated inhibition of the hippo pathway kinases Lats1 and 2 in the nucleus. Cancer Cell 2014; 26: 48–60. [PubMed: 25026211]
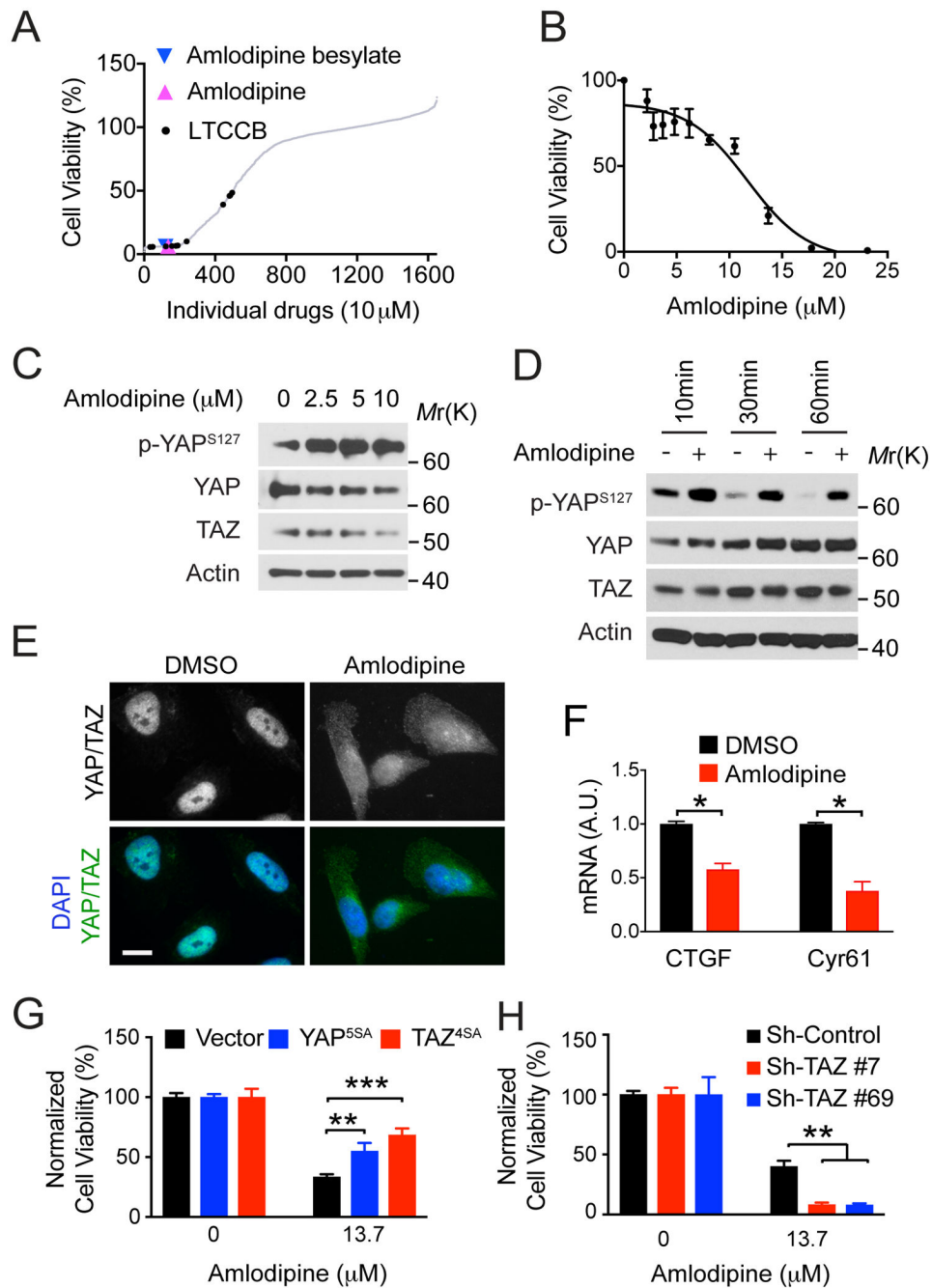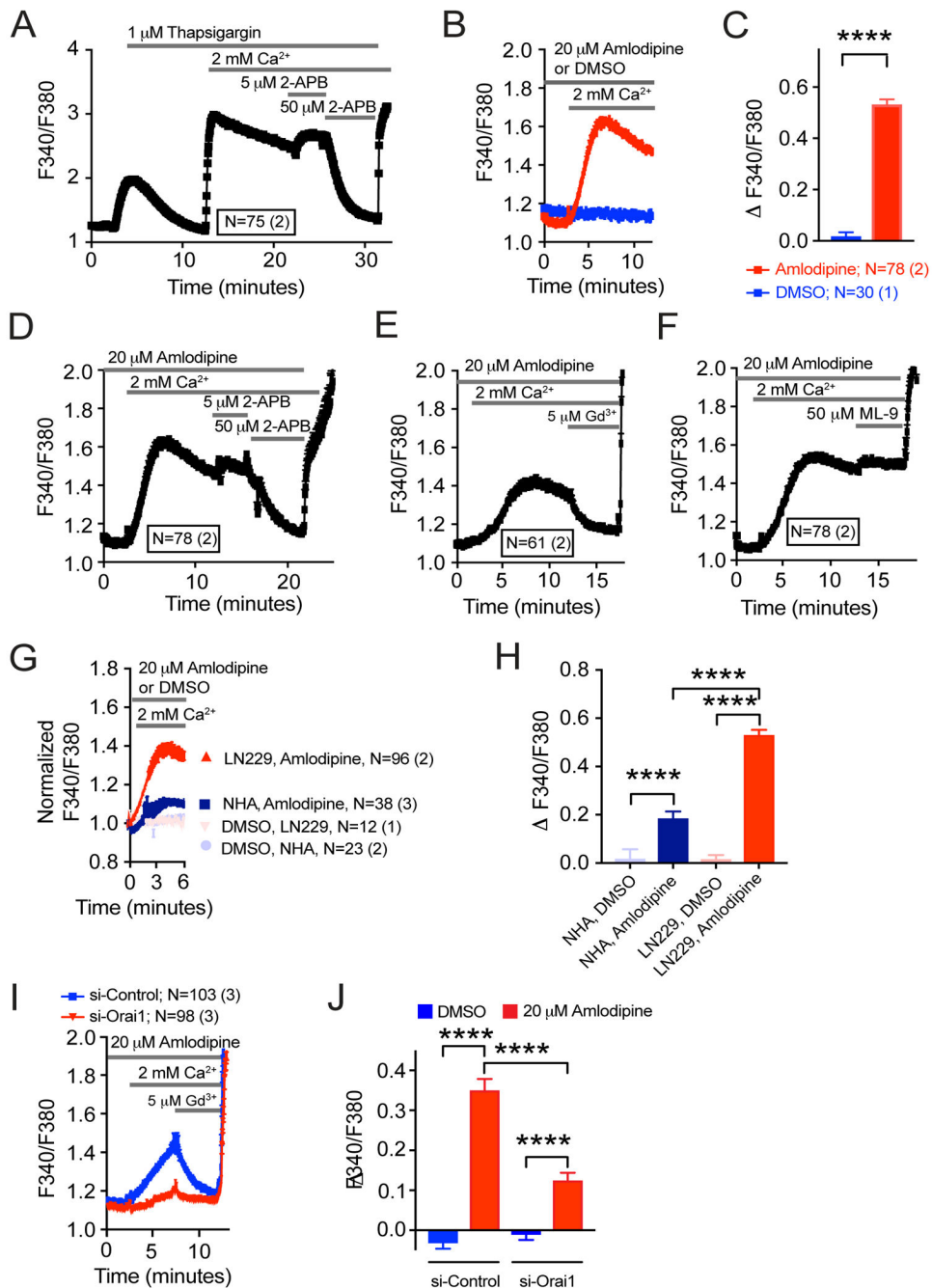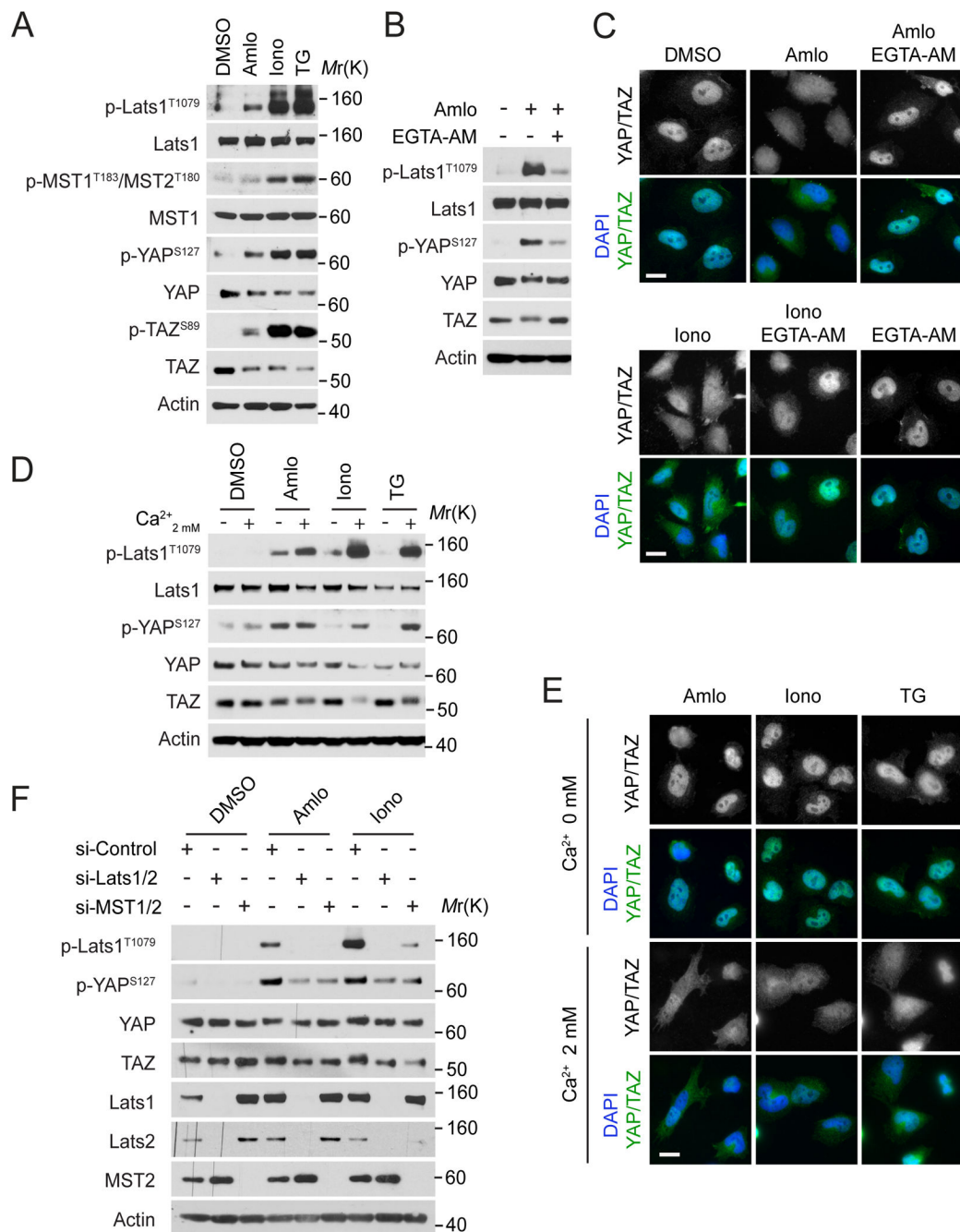
**Figure 1.**
Amlodipine inhibits cell survival and YAP/TAZ in LN229 cells. (A) An in vitro screen for small molecules, which inhibit LN229 cells, revealed the inhibitory effects of LCCB. (B) Cells were treated by amlodipine at indicated concentrations for three days and subjected to MTT assay. n=5. (C) Cells were treated by amlodipine at indicated concentrations for 24 hours and subjected to western blotting. Representative blots from three independent experiments. (D) Cells were treated with or without amlodipine (10μM) for indicated times and subjected to western blotting. Representative blots from three independent experiments.

(E) Cells were treated by DMSO or amlodipine for 30 minutes and subjected to IF staining. Representative images from three independent experiments. Scale bar =20 μm. (F) Cells were seeded in DMSO- or amlodipine-containing media for 3 hours and subjected to q-RT-PCR analysis. n=2. (G) and (H) Cells stably transduced by TAZ$^{4SA}$, YAP$^{5SA}$ or vector alone in (G), or by TAZ shRNAs or a scramble shRNA control in (H), were treated by DMSO or amlodipine for three days and subjected to MTT assay. In (G) and (H), the MTT reading of amlodipine-treated cells in indicated genetically modified groups were normalized to DMSO-treated cells in the correspondent groups. In (G), $n_{vector}$=6, $n_{YAP5SA}$=3, $n_{TAZ4SA}$=4. In (H), n=4. *P<0.05; **P<0.01; ***P<0.001.

**Figure 2.**
Amlodipine induces $Ca^{2+}$ entry in LN229 cells. (A) $Ca^{2+}$ measurements using the standard $Ca^{2+}$ off/ $Ca^{2+}$ on protocol and the dye Fura2-AM showing that 1 μM thapsigargin activated $Ca^{2+}$ release in nominally $Ca^{2+}$ free bath solutions and SOCE when extracellular $Ca^{2+}$ (2 mM) was replenished. Subsequent addition of 5 μM 2-APB potentiated SOCE while 50 μM 2-APB inhibited SOCE in LN229 cells. (B) and (C) In the absence of extracellular $Ca^{2+}$, 20 μM amlodipine did not activate a $Ca^{2+}$ signal. However, in the presence of extracellular $Ca^{2+}$, amlodipine activated significant and sustained $Ca^{2+}$ entry. (D) and (E) 50 μM 2-APB

and 5 μM $Gd^{3+}$ inhibited Amlodipine-activated calcium entry while 5 μM 2-APB potentiated $Ca^{2+}$ entry. (F) The SOCE inhibitor ML-9 (50 μM) which acts through disruption of STIM1 aggregation, did not inhibit amlodipine-activated $Ca^{2+}$ entry. (G) and (H) Amlodipine activated a significant $Ca^{2+}$ entry in both LN229 and NHA cells compared to vehicle control, DMSO. Compared to NHA cells, LN229 cells had significantly more amlodipine-activated $Ca^{2+}$ entry . (I) Knockdown of Orai1 substantially inhibited Amlodipine-activated $Ca^{2+}$ entry when compared to si-Control. Later addition of 5 μM $Gd^{3+}$ inhibited Amlodipine-activated $Ca^{2+}$ entry in both si-Control and si-Orai1 transfected cells. (J) Compared to vehicle, amlodipine activated significant $Ca^{2+}$ entry, and knockdown of Orai1 statistically inhibited Amlodipine-activated $Ca^{2+}$ entry when compared to si-Control. All data were derived from the indicated number of total cells and independent experiments detailed in outlined boxes. 10 μM ionomycin was included at the end of all tracings as a Fura2 loading control. ****$P<0.0001$

**Figure 3.**
Elevation of cytosolic $Ca^{2+}$ inhibits YAP/TAZ through the Hippo pathway in LN229 cells.
(A) Cells were treated by amlodipine (Amlo, 10 μM), Ionomycin (Iono, 1 μM), or
thapsigargin (TG, 1 μM) for 30 minutes and subjected to western blotting. Representative
blots from three independent experiments. (B) Cells were treated by Amlo (5 μM) with or
without EGTA-AM (12.5 μM) for 30 minutes and subjected to western blotting.
Representative blots from two independent experiments. (C) Cells were treated by Amlo (5
μM), Iono (0.5 μM) with or without EGTA-AM (12.5 μM) for 30 minutes and subjected to

IF staining. Representative images from two independent experiments. (D) and (E) Cells were treated in media with or without $Ca^{2+}$ containing Amlo (10 μM), Iono (1 μM), or TG (1 μM) for 30 minutes and subjected to western blotting (D) or IF staining (E). Representative blots and images from two independent experiments. (F) LN229 cells were transduced by siRNAs against Lats1 and Lats2 (Lats1/2), MST1 and MST2 (MST1/2) or scramble siRNA (control), treated by Amlo or Iono, and subjected to western blotting. Representative blots from three independent experiments. Scale bars =20 μm.
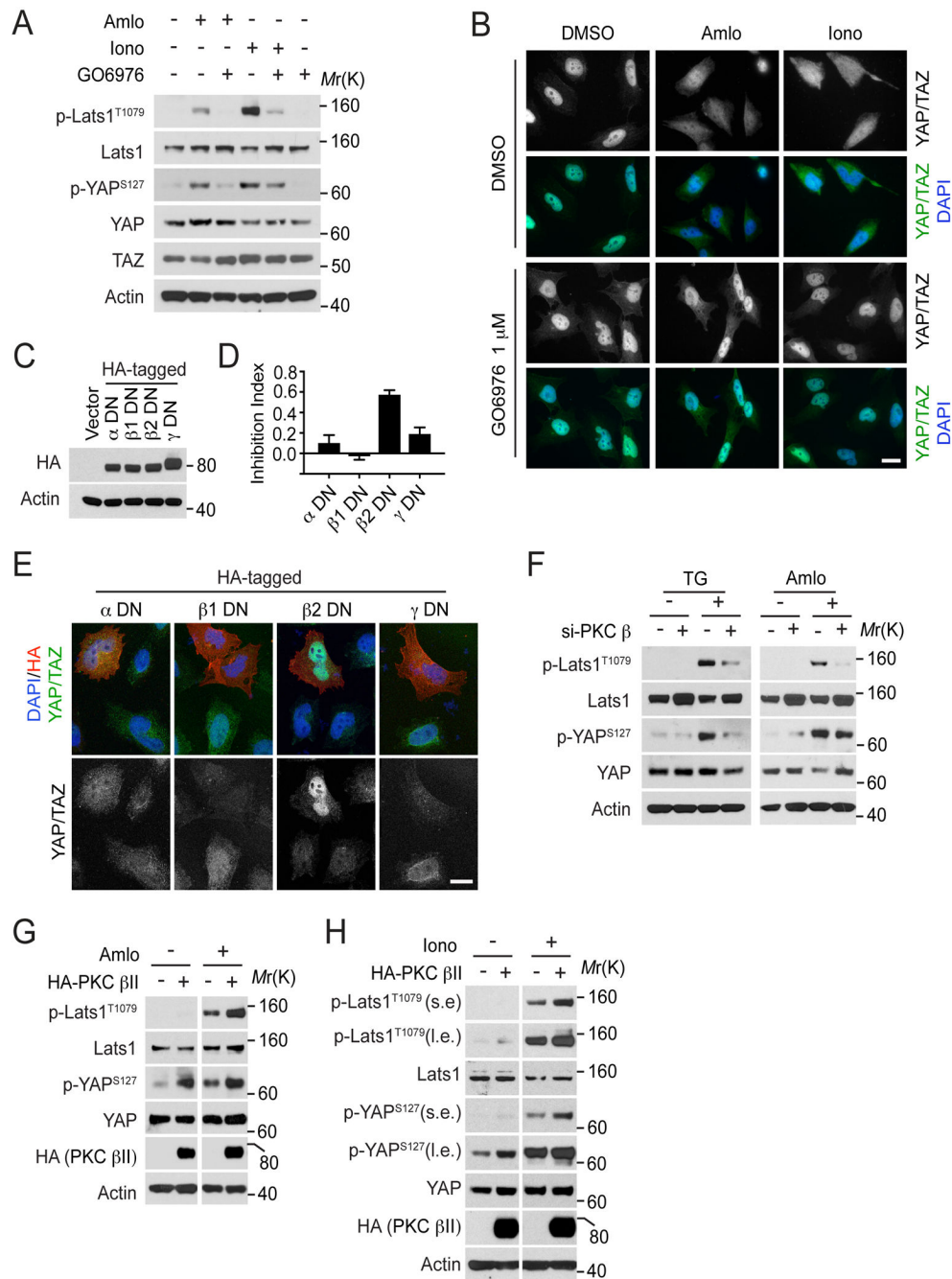
**Figure 4.**
cPKC mediates $Ca^{2+}$–induced Lats1 activation and YAP/TAZ inhibition in LN229 cells. (A) and (B) Cells were treated by Amlo or Iono with or without GO6976 (1 μM) and subjected to western blotting (A) or IF staining (B). Representative blots and images from three independent experiments. (C-E) Cells were transfected by indicated HA-tagged dominant negative (DN) mutants of individual cPKC isoenzymes, treated by amlodipine and subjected to western blotting (C) and IF staining (E) as indicated. Quantification of the effect of each PKC DN mutant on YAP/TAZ localization was shown in (D) (see methods). Representative

images from three (for beta II DN) or two (for the others) independent experiments. (F) Cells were transfected by siRNAs against PKC beta or scramble siRNA, treated by TG or Amlo, and subjected to western blotting. Representative blots from three independent experiments. (G) and (H) Cells transfected by HA-tagged PKC beta II were treated by Amlo (G), Iono (H) or DMSO as a control and subjected to western blotting. s.e., short exposure; l.e., long exposure. Representative blots from three independent experiments. Scale bar = 20 μm.
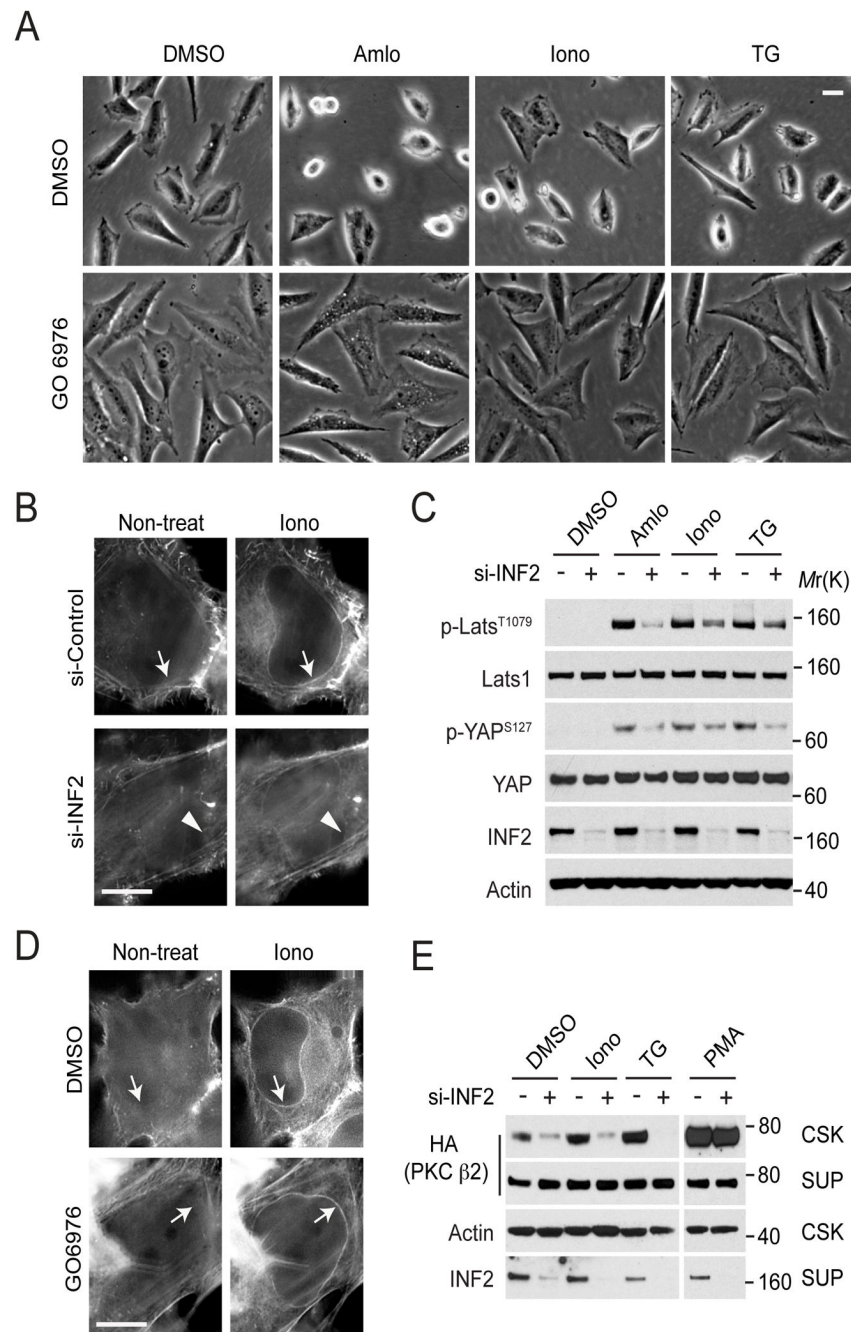
**Figure 5.**
INF2-mediated CaAR is required for $Ca^{2+}$-induced Hippo pathway activation and PKC beta II association with the actin cytoskeleton. (A) LN229 cells were treated by amlodipine, ionomycin or thapsigargin with or without GO6976 for 30 minutes and subjected to phase contrast imaging. Representative images from three independent experiments. Scale bar = 20 μm. (B) LN229 cells stably transduced by EGFP-Lifeact were transfected by siRNAs against INF2 or scramble siRNA, treated by ionomycin and subjected to live cell time-lapse imaging for EGFP. Representative images from 40 examined cells. Scale bar = 10 μm. (C) LN229

cells were transfected by siRNAs against INF2 or scramble siRNA, treated by amlodipine, ionomycin or thapsigargin and subjected to western blotting. Representative blots from two independent experiments. (D) LN229 cells stably transduced by EGFP-Lifeact were treated by ionomycin with or without GO6976 (1μM) and subjected to live cell time-lapse imaging for EGFP. Representative images from 40 examined cells. Scale bar =10 μm. (E) LN229 cells stably transduced by HA-tagged PKC beta II were transfected by siRNAs against INF2 or scramble siRNA, treated by ionomycin, thapsigargin or PMA for 20 minutes, and subjected to cytoskeletal fractionation into a Triton x100 soluble fraction (SUP) and insoluble cytoskeletal fraction (CSK), followed by western blotting. Representative blots from two independent experiments.
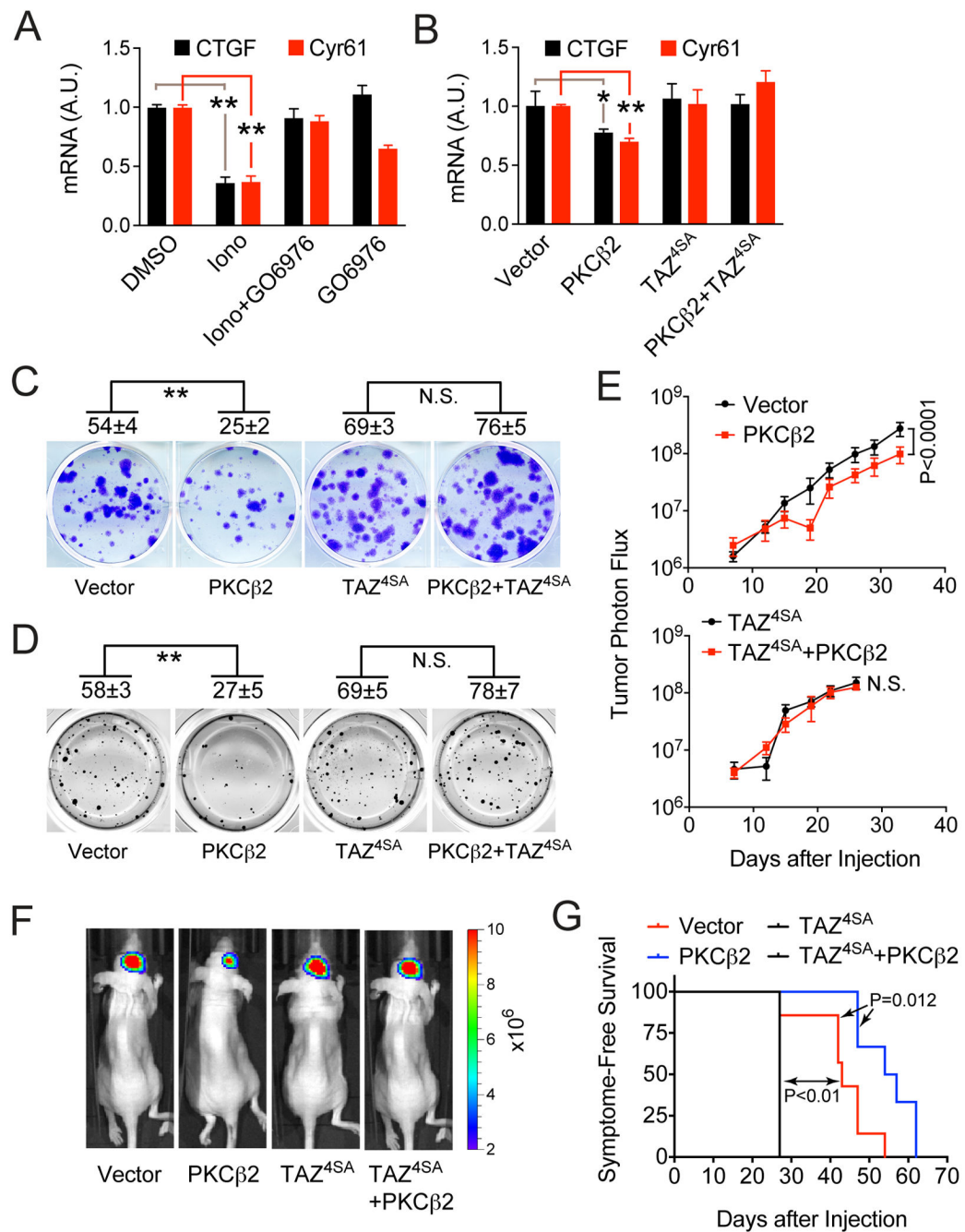
**Figure 6.**
PKC beta II inhibits YAP/TAZ-mediated transcription and GBM growth. (A) Cells were allowed to attach on petri dishes for 3 hours in media containing ionomycin with or without GO6976 (1 μM) followed by q-RT-PCR analysis for indicated gene expression. n=2, **P<0.01. (B) Cells stably transduced by indicated genes were allowed to attach on petri dishes for 3 hours followed by q-RT-PCR analysis for indicated gene expression. n=2, *P<0.05, **P<0.01. (C) and (D) Cells stably transduced by indicated genes were subjected to the colony formation assay (C) or the tumorsphere assay (D). Colonies (C) or spheres (D)

numbers in each well were counted and indicated. n=3, \*\*P<0.01. N.S., P>0.05. (E) Cells expressing luciferase were transduced by indicated genes, followed by intracranial injection into nude mice. Tumors were monitored by bioluminescence imaging. n=6 for vector, n=7 for PKC beta II, n=5 for TAZ$^{4SA}$ and n=5 for TAZ$^{4SA}$+PKC beta II. The P values at day 33 were shown. 2-way ANOVA was used in this case. N.S., P>0.05. (F) Represent mice bioluminescence imaging at Day 26 from (E) were shown. (G) Survival curves were shown from the mice in (E) and Logrank tests were performed.
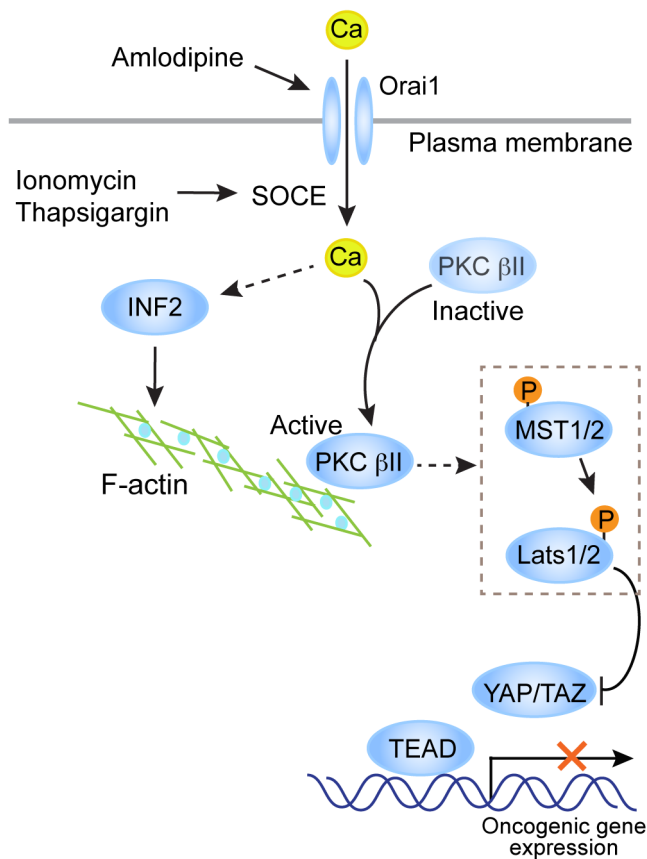
**Figure 7.**
Model illustrating the mechanism by which $Ca^{2+}$ inhabits YAP/TAZ-mediated transcriptional program. Elevation of cytosolic $Ca^{2+}$ by indicated approaches induces INF2-mediated actin cytoskeleton remodelling, which leads to new actin-filament assembly. At the same time, $Ca^{2+}$ induces PKC beta II translocation to the newly formed F-actin compartment, where PKC beta II is activated. Active PKC beta II induces activation of the core Hippo kinase cascade, including MST1/2 and Lats1/2 phosphorylation. Lats1/2 then phosphorylate YAP/TAZ and shut down the downstream transcriptional program of oncogenic genes.